ACS APPLIED MATERIALS & INTERFACES

Research Article

www.acsami.org

Engineered Stealth Porous Silicon Nanoparticles via Surface Encapsulation of Bovine Serum Albumin for Prolonging Blood Circulation in Vivo

Bing Xia,*[,†] Wenyi Zhang,[†] Jisen Shi,[†] and Shou-jun Xiao[‡]

[†]Key Laboratory of Forest Genetics & Biotechnology (Ministry of Education of China), Advanced Analysis & Testing Center, Nanjing Forestry University, Nanjing 210037, P. R. China

[‡]Nanjing National Laboratory of Microstructures, School of Chemistry and Chemical Engineering, Nanjing University, Nanjing 210093, P. R. China

Supporting Information

ABSTRACT: Luminescent porous silicon nanoparticles (PSiNPs) have been widely used as drug delivery. However, fast biodegradation and short blood circulation have been major challenges for their biomedical applications. Herein, bovine serum albumin was readily encapsulated onto alkyl-terminated PSiNPs surfaces via hydrophobic interaction, which could significantly improve their water-dispersibility and long-term stability under physiological conditions. Furthermore, compared with PSiNPs alone, PSiNPs coated with bovine serum albumin remarkably reduced nonspecific cellular uptake in vitro and prolonged blood circulation in vivo.

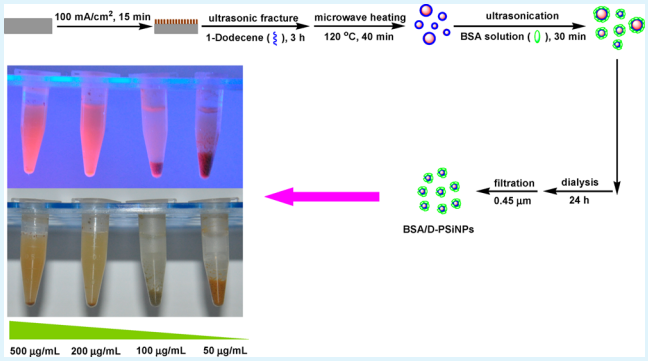

KEYWORDS: *porous silicon, nanoparticles, BSA encapsulation, cellular uptake, blood circulation*

1. INTRODUCTION

Luminescent porous silicon nanoparticles (PSiNPs) exhibited a considerable potential for cancer treatments in vivo, such as tumor imaging,[1−3] anti-cancer drug delivery,[1,4−7] photodynamic therapy,[8] and thermotherapy,[9,10] which was due to their versatile physicochemical properties (e.g., strong fluorescence, biocompatibility, surface tailorability, tunable porous nanostructure, and the ability to support cell growth). PSiNPs could also be easily degraded in biological environments to form nontoxic silicic acid, which provided a pathway for their safe clearance from the body.[1,11−15] However, in buffer or culture media, fast biodegradation of PSiNPs spontaneously resulted in fluorescence quenching, which limited their application on long-term tumor imaging. For example, if incubated in phosphate buffered saline solution (PBS, pH 7.4) at 37 °C, bare PSiNPs lost 67% of their luminescence after 1 h, and no detectable luminescence remained after 8 h.[1] After intravenous injection, a large fraction of bare PSiNPs could be degraded into smaller nanoparticles (<5.5 nm).[1] And then like most foreign nanomaterials in vivo, they were often rapidly recognized and scavenged from the bloodstream by the cells of the reticuloendothelial system (RES), which limited circulation time of PSiNPs in vivo.

Long blood circulation time of PSiNPs as drug carriers was desired to improve the efficient delivery of the payload to the target site after intravenous administration. To enhance the blood circulation time of PSiNPs, various surface coatings of PSiNPs had been fabricated to retard their biodegradable rate, such as, undecenoic acid grafted by hydrosilylation,[12,14−16] silica coated by sol-gel process,[13] or biopolymer dextran modified by physisorption.[1] In our previous work, we found that PSiNPs modified with 10-undecenoic acid via microwave-induced hydrosilylation showed excellent fluorescence stability under physiological conditions.[17,18] As another strategy to prolong blood circulation time, the preparation of "stealth" nanoparticles with surface modification of polyethylene glycol or zwitterionic polymer, which could dramatically resist protein adsorption and minimize clearance by the renal system.[19−26] In addition, surface coating of bovine serum albumin (BSA, an important blood protein) was also proved to effectively minimize recognition and internalization by macrophages, and then evade immune attack in the body.[27,28] Mirkka S. et al. ever reported that thermally hydrocarbonized PSiNPs were biofunctionalized with a self-assembled fungal hydrophobin protein coating via hydrophobic interaction, which efficiently improved their water-dispersibility and resulted in significant alteration in their accumulation to the liver and spleen.[29] Except for this reference, few other reports about similar stealth PSiNPs had been found. Herein, we presented a general strategy for encapsulating bovine serum albumin (BSA, an

Received: August 13, 2013
Accepted: October 19, 2013
Published: October 20, 2013

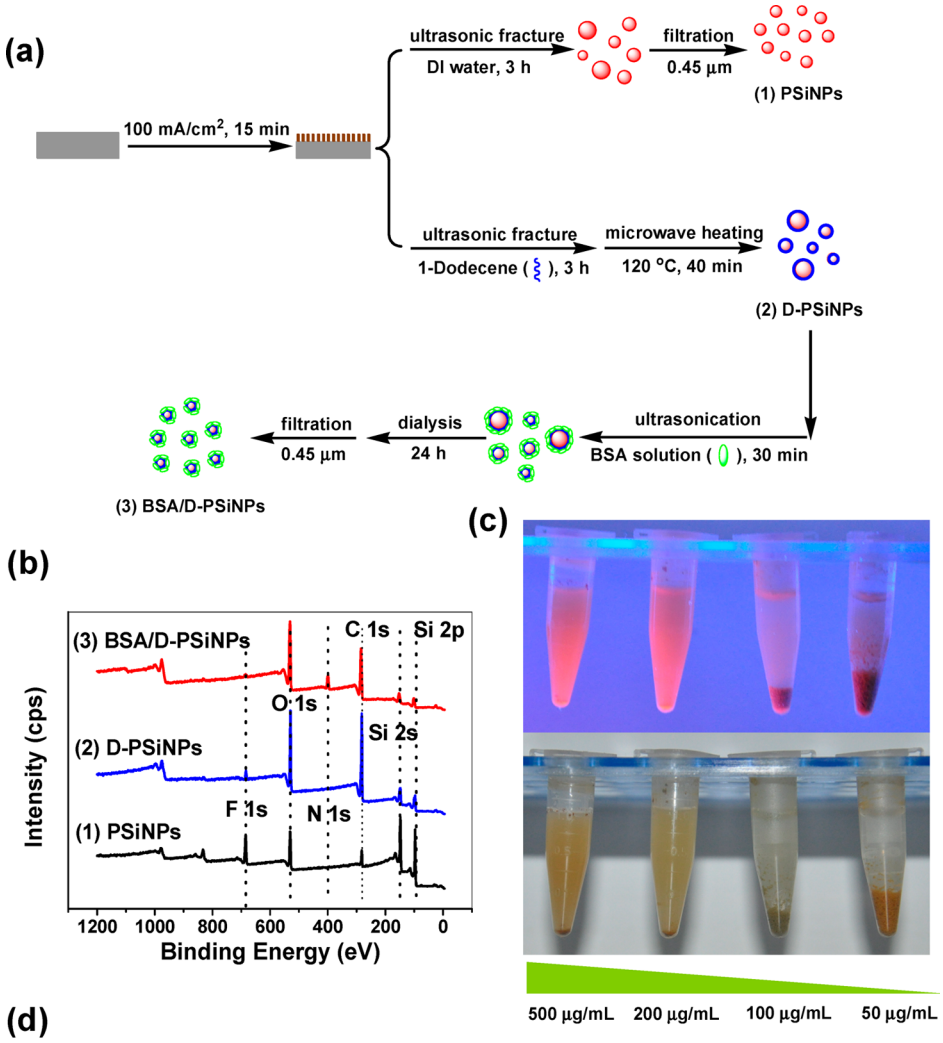

(d)

Materials	Mass Concentration (%)					
	C 1s (285 eV)	N 1s (400 eV)	O 1s (532 eV)	Si 2p (103 eV)	Si 2s (154 eV)	F 1s (685 eV)
PSiNPs	6.22	0.00	8.78	35.42	42.55	7.03
D-PSiNPs	41.22	0.00	17.00	18.07	22.16	1.55
BSA/D-PSiNPs	37.82	6.92	23.88	14.82	15.50	1.07

Figure 1. (a) Schematic diagram of microwave-assisted synthesis of D-PSiNPs and BSA encapsulation, (b) XPS survey of bare PSiNPs, dodecene grafting, and BSA encapsulation, (c) the corresponding table of atomic concentrations, and (d) the CCD images of D-PSiNPs dispersed in BSA solutions with various concentration (50, 100, 200, and 500 μg/mL) under ambient light (bottom) and 360 nm UV lamp (top).

important blood protein) onto alkyl-terminated PSiNPs via hydrophobic interaction (shown in Figure 1a), which could significantly improve their water-dispersibility and long-term fluorescence stability under physiological conditions. Compared with PSiNPs alone, these BSA-coated PSiNPs remarkably reduced nonspecific cellular uptake in vitro and prolonged blood circulation in vivo. These above-mentioned results demonstrated that as-prepared stealthy PSiNPs as drug carriers or fluorescence probes would have a great potential on biomedical applications in vivo.

2. EXPERIMENTAL SECTION

2.1. Preparation of PSiNPs. The single side polished, (100) oriented, and p-type silicon wafers (boron doped, 8−10 Ω cm resistivity, purchased from Hefei Kejing Materials Technology Co. Ltd., China) were boiled in 3:1 (v/v) concentrated H_2SO_4/30% H_2O_2 for 30 min and then rinsed copiously with Milli-Q water (≥18 MΩ cm resistivity). The porous silicon (PSi) samples (1.54 cm^2) with about 30 μm thick porous layer were prepared by electrochemically etching in an ethanolic HF solution (40% HF/ethanol (1:1 v/v)) at 20 mA/cm^2 for 45 min. After the sonication in water to detach the porous layer and filtration with 0.45 μm filtration membrane, PSiNPs samples were prepared for next experiments.

2.2. Synthesis of BSA-Coated PSiNPs. The single-mode heating microwave system NOVA made by Preekem of Shanghai in China was

used for the microwave-assisted synthesis of carboxyl-terminated PSiNPs (UA-PSiNPs) and alkyl-terminated PSiNPs (D-PSiNPs). The fresh prepared PSi samples were immersed in pure 1-dodecene, followed by sonication and 40-min microwave heating at 120 °C. Using 30 min centrifugation at 1.2 × 10^5 rpm, the samples were washed by ethanol to obtain D-PSiNPs. After 30 min sonication in 200 μg/mL BSA solution, 24 h dialysis in water (100 000 Da molecular weight cut-off), and filtration with 0.45 μm filtration membrane, BSA-coated PSiNPs (BSA/D-PSiNPs) were prepared for next experiments. The fresh prepared PSi samples were also immersed in pure 10-undecenoic acid, followed by sonication and microwave irradiation. After 40-min heating at 120 °C, 24 h dialysis in water (60 000 Da molecular weight cut-off), and filtration with 0.45 μm filtration membrane, UA-PSiNPs were prepared for next experiments.

2.3. Cell Viability Assays in Vitro. Hela cells (~3 × 10^5 cell/mL) were dispersed within 96-well plates to a total volume of 100 μL/well and maintained at 37 °C in a 5% CO_2/95% air incubator for 24 h. Then the culture media was removed and the cells were incubated in culture medium containing the as-prepared PSiNPs, UA-PSiNPs, or BSA/D-PSiNPs with different concentrations for 24 h and washed with the culture medium. An amount of 100 μL of the new culture medium containing 3-(4,5-dimethylthiazol-2-yl)-2,5-diphenyltetrazolium bromide (MTT) (10 μL, 5 mg/mL) was then added, followed by incubating for 4 h to allow the formation of formazan dye. After removing the medium, 150 μL DMSO was added to each well to dissolve the formazan crystals. Absorbance was measured at 570 nm in a microplate photometer. Cell viability values were determined (at least three times) according to the following formulae: cell viability (%) = the absorbance of experimental group/the absorbance of blank control group ×100%.

2.4. Nonsepcific Cellular Uptake Test in Vitro. Hela cells were plated onto 30-mm cell culture coverslips and incubated with 20 μg/mL UA-PSiNPs (or BSA/D-PSiNPs) for 24 h. The attached nanoparticles were washed three times with PBS solution (pH 7.4), and cells samples were monitored using laser scanning confocal microscopy (LSCM) (Leica TCS SP5, Germany) with the excitation at 405 nm. For transmission electron microscopy (TEM) analysis of cell sections, the cells were seeded on a 6-well plate at a certain density (~5 × 10^5 cell/mL) and cultured for 24 h. Then the cells were incubated with 20 μg/mL UA-PSiNPs (or BSA/D-PSiNPs) for 12 h. At a determined time, the cells were washed five times with PBS and trypsinized, centrifuged, and then fixed with 2.5% glutaraldehyde. After 2 h fixation at 4 °C, the samples were washed with PBS solution three times. Then the samples were fixed with 1% perosmic oxide for 2 h at 4 °C. After being washed in water, the samples were dehydrated in an alcohol series, embedded, and sliced with thickness from 50 to 70 nm.

2.5. Blood Circulation Test in Vivo. Six week old balb/c mice were used in our study. PSiNPs, UA-PSiNPs, and BSA/D-PSiNPs (in 200 μL PBS solution) were intravenously injected into the tail vein of each mouse at a dose of 20 mg/kg body mass. To determine blood half-lives, we collected the blood (100 μL) from the tail vein at several different times after injection using heparinized capillary tubes (Fisher), and then immediately mixed it with 100 μL of 10 mM EDTA (in PBS) to prevent coagulation. The total silicon concentration in the blood was measured using inductively coupled plasma mass spectrometry (ICP-MS).

2.6. Instruments and Methods. UV−vis adsorption spectra were recorded by a Shimadzu UV-2450 spectrophotometer. PL measurements were performed using a Perkin-Elmer LS55 fluorescence spectrometer. X-ray photoelectron spectra (XPS) were recorded using Kratos AXIS Ultra DLD system with a monochromatic Al Kα X-ray beam (1486.6 eV) at 150 W in a residual vacuum of <4 × 10^{-9} Pa. Analysis of nanoparticles size and surface charge was performed using Malvern Zetasizer Nano ZS dynamic-light-scattering (DLS) measurements. Scanning electron microscopy (SEM) images were taken by JEOL JSM-7600F scanning electron microscope with the accelerating voltage of 15 kV. TEM images were taken by JEOL JEM-2100 UHR transmission electron microscope with the accelerating voltage of 200 kV. Multiscan MK3 microplate photometer (Thermo Scientific) was used to monitor the absorbance of Hela cells during MTT assays. Silicon concentration in blood samples was determined by ICP-MS (PerkinElmer NexION 300). Elemental analysis (C, H, and N) were performed on Elemental Vario Micro analyzer (Germany).

3. RESULTS AND DISCUSSION

3.1. Design, Synthesis, and Characterizations of BSA/D-PSiNPs. Because of high affinities for hydrophobic or charged surfaces, proteins could be readily adsorbed onto nanoparticles, and then formed a corona outside nanoparticles, which would interact with cellular receptors and define the fate of nanoparticles in a biological environment.[30,31] In our experiments (seen in Figure 1a), 1-dodecene was grafted onto the surfaces of PSiNPs by microwave-induced hydrosilylation to prepare D-PSiNPs with higher hydrophobicity. And then D-PSiNPs was dispersed in BSA solutions with different concentration (50, 100, 200, and 500 μg/mL) by ultrasonication. As seen in Figure 1c, the water-dispersibility of D-PSiNPs could be improved by increasing BSA concentration. When BSA concentration reached 200 μg/mL, D-PSiNPs was almost homogeneously dispersed in solution, and showed a strong orange red fluorescence under UV irradiation. We suggested that amphiphilic BSA could be efficiently encapsulated onto D-PSiNPs via hydrophobic interaction, whereas the large amount of hydrophilic carboxyl or amino groups of adsorbed BSA could enhance the aqueous solubility of D-PSiNPs. Microwave-assisted synthesis of D-PSiNPs and subsequent BSA encapsulation were also stepwise monitored by XPS. The survey spectra of PSiNPs (**1**), 1-dodecene grafting (**2**) and BSA encapsulation (**3**) were displayed in Figure 1b. The signals of C 1s (285 eV), N 1s (400 eV), O 1s (532 eV), Si 2p (103 eV), Si 2s (154 eV), and F 1s (685 eV) were detected, which was consistent with the incorporation of organic molecules on PSiNPs. And the corresponding atomic concentrations of these elements were calculated in Figure 1d. Carbon concentration changed as (**1**) (6.22%) → (**2**) (41.22%) → (**3**) (37.82%), which indicated that it clearly increased after grafting 1-dodecene with long alkyl chains. Nitrogen concentration was also informative in our system because of its rich content in proteins. It evolved as (**1**) (0.00%) → (**2**) (0.00%) → (**3**) (6.92%), which exhibited that N 1s signal was easily detected on (**3**) because of the rich nitrogen in BSA. Oxygen concentration increased as (**1**) (8.78%) → (**2**) (17.00%) → (**3**) (23.88%), because of the microwave-induced oxidation from (**1**) to (**2**) and ultrasonication-induced oxidation in water from (**2**) to (**3**). The atomic concentration of silicon and fluorine (residue from HF etching) gradually decreased during the process of 1-dodecene attachment and BSA encapsulation. The increasing of thickness of surface coatings led to a decrease of the depth of silicon and fluorine detected by X-ray, therefore, the intensity of Si 2s, Si 2p, and F 1s signals would become weaker. The surface coverage of attached ligands on D-PSiNPs and BSA/D-PSiNPs was determined by elemental analysis of nitrogen or carbon (Table S1 in the Supporting Information). According to the method reported in ref 32, the amount of grafted 1-dodecene on D-PSiNPs was calculated as 0.82 mmol/g, and the amount of grafted BSA on BSA/D-PSiNPs was calculated as 0.72 μmol/g. According to these above-mentioned characterizations, BSA had been successfully encapsulated onto alkyl-terminated surfaces of PSiNPs, which efficiently improved their aqueous solubility.

After excess BSA and large nanoparticles were removed using dialysis and filtration, the milky white solution of BSA/D-

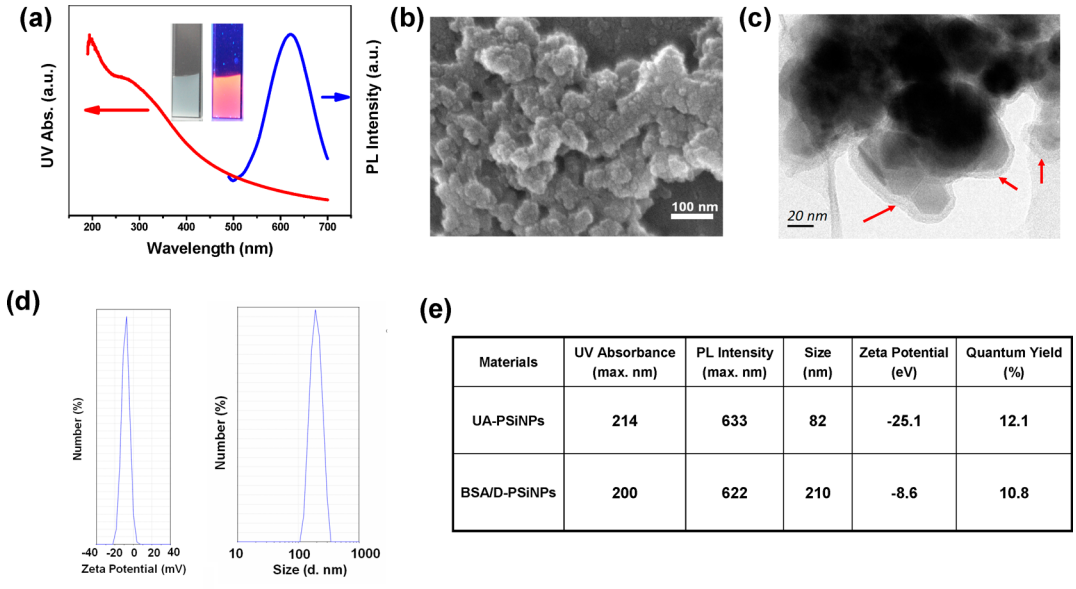

(e)

Materials	UV Absorbance (max. nm)	PL Intensity (max. nm)	Size (nm)	Zeta Potential (eV)	Quantum Yield (%)
UA-PSiNPs	214	633	82	-25.1	12.1
BSA/D-PSiNPs	200	622	210	-8.6	10.8

Figure 2. (a) UV−vis and PL spectra of BSA/D-PSiNPs, and its corresponding CCD images under ambient light (left) and 360 nm UV lamp (right) (in the insert), (b) SEM image of BSA/D-PSiNPs, (c) TEM image of BSA/D-PSiNPs, (d) the representative DLS histogram of BSA/D-PSiNPs in water, and (e) the table of characterizations of BSA/D-PSiNPs and UA-PSiNPs.

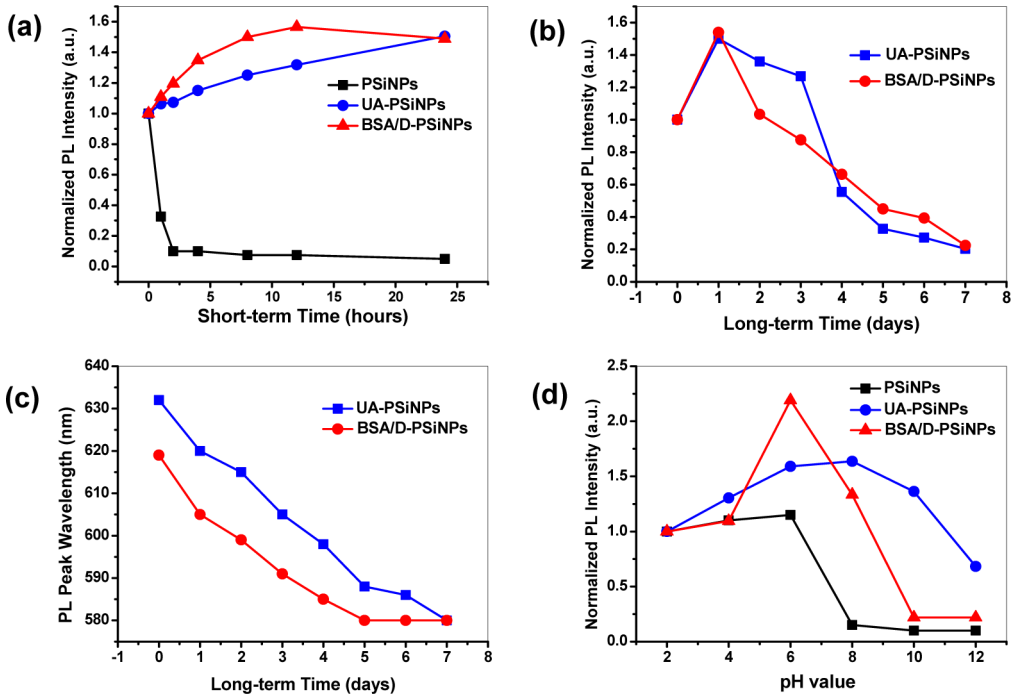

Figure 3. (a) PL intensity with time (hours) of PSiNPs, UA-PSiNPs, and BSA/D-PSiNPs in PBS solution (pH 7.4) at 37 °C, respectively; (b) PL intensity with time (days) of UA-PSiNPs and BSA/D-PSiNPs in PBS solution (pH 7.4) at 37 °C; (c) PL wavelength with time (days) of UA-PSiNPs and BSA/D-PSiNPs in PBS solution (pH 7.4) at 37 °C; and (d) PL intensity with pH value of PSiNPs, UA-PSiNPs, and BSA/D-PSiNPs in water at room temperature, respectively.

PSiNPs with excellent stability could be prepared, which still retained the distinct orange red luminescence under UV irradiation (shown in the insert of Figure 2a). SEM and TEM measurements were utilized to observe the size and morphology of BSA/D-PSiNPs, and are shown in images b and c in Figure 2. According to SEM images, we found that the nanostructures in the range of 10−100 nm were not individual nanocrystals, but were silicon nanoparticle domains trapped in larger pieces of the porous silicon structure.[1,16−18] From TEM images, BSA layer surrounding PSiNPs (marked by red arrows) with the depth of 10−20 nm was obviously observed. In d and e in Figure 2, the mean hydrodynamic size of BSA/D-PSiNPs measured by DLS was ∼210 nm, which was larger than that of UA-PSiNPs (∼82 nm). We suggested that after thin BSA layers (∼20 nm) coated onto PSiNPs, these nanoparticles would be aggregated to form larger size particles via BSA crosslinking in the solution. And compared with UA-PSiNPs (-25.1 mV), BSA/D-PSiNPs held lower zeta potential (−8.6 mV), which

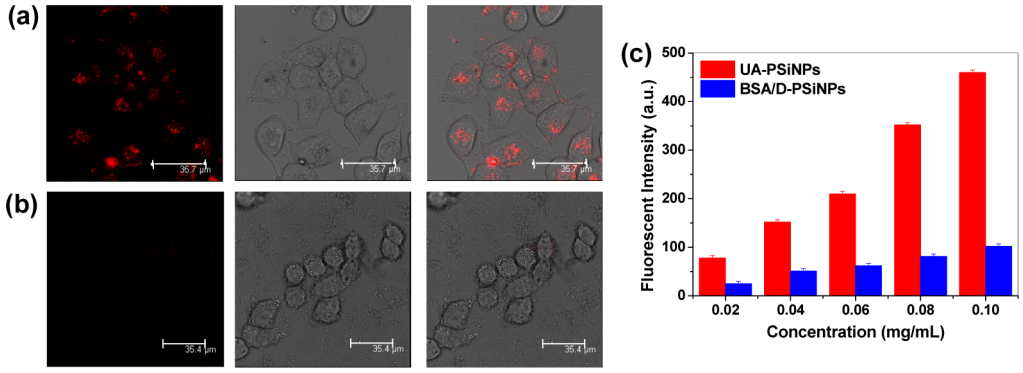

Figure 4. Typical LSCM images of Hela cells after the uptake of (a) 20 μg/mL UA-PSiNPs and (b) 20 μg/mL BSA/D-PSiNPs (from left to right: fluorescence channel, bright-field channel, and the overlay). (c) Histogram of intracellular mean fluorescence intensity of UA-PSiNPs and BSA/D-PSiNPs with varied concentrations at different incubation times.

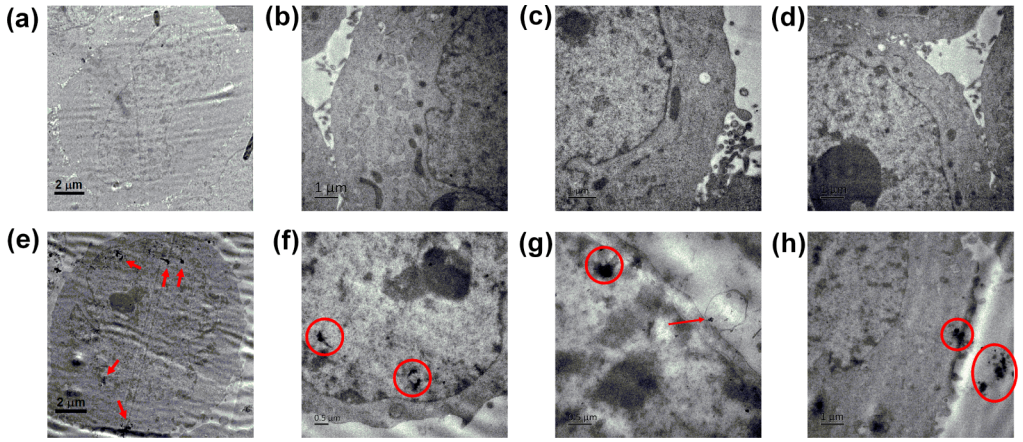

Figure 5. Typical TEM images of Hela cells after the uptake of (a–d) 20 μg/mL BSA/D-PSiNPs, and (e–h) 20 μg/mL UA-PSiNPs (nanoparticles internalized by cells marked by red arrow or circles).

was in accordance with the surface charge of BSA coating.[33] In our previous work, we found that a traditional EDC/NHS method in alkali reaction conditions (pH >9) for protein immobilization onto porous silicon surfaces generally resulted in the heavy degradation of nanostructures.[34,35] However, this simple strategy of BSA encapsulation via hydrophobic interaction could efficiently avoid the biodegradation of PSiNPs.

Moreover, the optical properties of BSA/D-PSiNPs were characterized by UV–vis and PL spectra. As seen in Figure 2a, the normalized UV-PL spectra of BSA/D-PSiNPs indicated that they possessed good PL properties with clearly resolved emission peak (λ_{em} = 622 nm). Using Rhodamine 101 as a standard,[1,17,18] the fluorescence quantum yield of BSA/D-PSiNPs in ethanol was determined to be ~10.8%. Degradation of PSiNPs could be monitored by their fluorescence quenching, thus we recorded PL spectra of BSA/D-PSiNPs under physiological conditions in Figure 3a–c. Bare PSiNPs and UA-PSiNPs had been systematically studied in our previous work.[17] According to Figure 3a and Figure S1 in the Supporting Information, the fluorescence of bare PSiNPs in PBS solution (pH 7.4) at 37 °C was completely quenched after only 2 h. In contrast, the PL intensity of UA-PSiNPs gradually increased, reaching ~150% of the initial intensity after 24 h of incubation. Similar phenomenon of fluorescence activation had been also observed in BSA/D-PSiNPs, which was attributed to quantum confinement effects and defects localized at the Si-SiO_2 interface.[1,15,17] On a longer time scale (days) incubation, the PL characteristics of BSA/D-PSiNPs were recorded in panels b and c in Figure 3, and Figure S2 in the Supporting Information. With a constant blueshift in PL emission, the fluorescence of BSA/D-PSiNPs remained stable within 3 days and lost 80% after 7 days, which was attributed to their slow degradation in PBS solution at 37 °C. Additionally, the pH stability of BSA/D-PSiNPs was also measured in acidic-to-basic environments (pH 2–12) (shown in Figure 3d and Figure S3 in the Supporting Information). The fluorescence of bare PSiNPs was completely quenched in alkaline solution (pH 8). However, the PL intensity of UA-PSiNPs slightly decreased by ~20% within pH 4-10, and the PL intensity of BSA/D-PSiNPs decreased by ~50% within pH 4-8. On the whole, UA-PSiNPs > BSA/D-PSiNPs > bare PSiNPs in order of fluorescence stability could be found, which confirmed that surface coatings (whether BSA layers or UA films) could provide a protective shell to retard the biodegradation of PSiNPs. And the stability of UA-PSiNPs was superior to that of BSA/D-PSiNPs in physiological environments was due to dense 10-undecenoic acid monolayers via thermal stable covalent bonding.

3.2. Nonsepcific Cellular Uptake of BSA/D-PSiNPs. To study the nonspecific cellular uptake of BSA/D-PSiNPs, we first incubated Hela cells with the 20 μg/mL BSA/D-PSiNPs (and UA-PSiNPs as a control) in PBS solution (pH 7.4) at 37 °C for 24 h, washed them with PBS solution, and then observed with LSCM. In Figure 4a, with the excitation at 405 nm, an intense

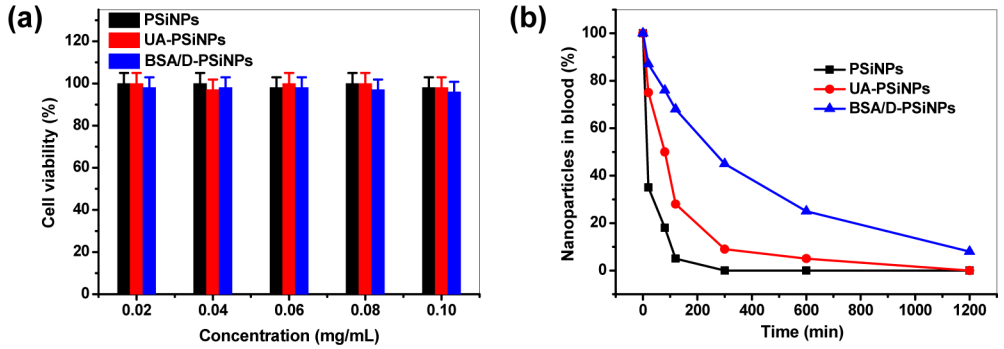

Figure 6. (a) Cytotoxicity of bare PSiNPs, UA-PSiNPs, and BSA/D-PSiNPs with different concentrations toward Hela cells. (b) Blood concentration of silicon for mice injected with bare PSiNPs, UA-PSiNPs, and BSA/D-PSiNPs as a function of time.

fluorescence signal caused by UA-PSiNPs could be seen in intracellular compartments of Hela cells, which showed that they had a good cell-permeability and maintained their PL characteristics in intracellular environments. However, after the incubation with BSA/D-PSiNPs, negligible fluorescence signal could be detected in Hela cells in Figure 4b. Furthermore, BSA/D-PSiNPs (or UA-PSiNPs) with different concentrations were co-cultured with Hela cells, and average cellular fluorescence intensity of 50 cells from these samples were analyzed by LAS AF Lite software. As illustrated in Figure 4c, the cellular uptake of these nanoparticles was observed to be concentration-dependent, whether UA-PSiNPs or BSA/D-PSiNPs. By comparing BSA/D-PSiNPs with UA-PSiNPs, we found that BSA/D-PSiNPs could greatly minimize the uptake of Hela cells. As well as the quantitative fluorescence measurement, the internalization of PSiNPs into cells was also evaluated by TEM imaging. Because of the resistance of uptake of BSA/D-PSiNPs by Hela cells, even carefully checking more than 30 cells for each cell section sample, no nanoparticles were observed in cells (shown in Figure 5a–d). In contrast, UA-PSiNPs were clearly detected in Hela cells, as seen in Figure 5e–h. From these TEM images, UA-PSiNPs were mainly trapped in the nucleus as aggregates, which was also consistent with the results of LSCM measurements. The cellular internalization of porous silicon nano or micro-particles with different sizes (from ~4 nm to ~2 μm) had been repeatedly reported,[1,36,37] which demonstrated that the size effect was not the key factor on the cellular uptake of PSiNPS. Accordingly, we suggested that amphiphilic BSA coating layer on PSiNPs is the key factor to resist nonspecific uptake of Hela cells.

3.3. Cell Viability and Blood Circulation of BSA/D-PSiNPs. Before in vivo experiments, MTT assays were adopted to evaluate the cytotoxicity of PSiNPs, UA-PSiNPs and BSA/D-PSiNPs to Hela cells in dark. Cell viability of these nanoparticles with different concentrations (20, 40, 60, 80, and 100 μg/mL) had been investigated in Figure 6a. These results displayed that PSiNPs, UA-PSiNPs and BSA/D-PSiNPs produced negligible cytotoxicity to Hela cells after 24 h of incubation in dark. The cytotoxicity of silicon particles has been studied in vitro or in vivo, which showed that the main reason is the reactive oxygen radical generated by silicon nanostructures.[37−41] For PSiNPs, photoinduced reactive oxygen radical was also found as the main pathway to produce their cytotoxicity.[8,42,43] However, according to our previous study and others references,[1,8,16,18,44] low concentration (< 0.1 mg/mL), and the incubation in dark could efficiently avoid the cytotoxicity of PSiNPs, which was attributed to favorable biocompatibility of silicon.

Sufficient blood circulation time was critical to in vivo applications of PSiNPs, including tumor imaging, targeting, and therapy. We also examined blood circulation time of PSiNPS, UA-PSiNPs and BSA/D-PSiNPs after intravenous administration. According to Figure 6b, the BSA-coated PSiNPs exhibited longer blood circulation (half-life ~262.4 min) than that of UA-PSiNPs (~86.2 min) and bare PSiNPs (~28.6 min). These results confirmed that without surface modification, a large fraction of the bare PSiNPs would be immediately removed by renal clearance, presumably owing to their degradation into smaller nanoparticles. After whether BSA coating or UA grafting, the blood half-life time of PSiNPs increased by preventing their biodegradation. Additionally, serum albumin were considered to so-called dysopsonins that could potentially prevent the opsonization process from occurring and possibly increase the circulation time of the nanoparticle. Compared with 10-undecenoic acid films, the outmost BSA layers also made a "stealth" surface on PSiNPs, which effectively reduced nonspecific cellular uptake in vitro and prolonged blood circulation time by avoiding the RES uptake in vivo.

4. CONCLUSION

In conclusion, a general method for BSA coating onto PSiNPs surfaces via hydrophobic interaction was developed, which could afford high aqueous solubility and long-term stability under physiological conditions. Moreover, the BSA-coated PSiNPs could significantly minimize the nonspecific cellular uptake, and exhibit longer blood circulation upon intravenous injection into mice. The long blood circulation time suggested greatly delayed clearance of nanomaterials by the RES of mice, a highly desired property for in vivo applications of nanomaterials, including tumor imaging and drug delivery. So these resultant BSA/D-PSiNPs with excellent biocompatibility would have a great potential on in vivo applications as fluorescence probes or drug delivery.

■ ASSOCIATED CONTENT

Supporting Information

PL spectra of BSA/D-PSiNPs incubated in aqueous solution under different conditions, elemental analysis of D-PSiNPs and BSA/D-PSiNPs, and CCD images of D-PSiNPs and BSA/D-PSiNPs incubated in a dual-phase solution of H_2O/CH_2Cl_2. This material is available free of charge via the Internet at http://pubs.acs.org/.

AUTHOR INFORMATION

Corresponding Author

*E-mail: xiabing@njfu.edu.cn.

Notes

The authors declare no competing financial interest.

ACKNOWLEDGMENTS

This work is funded by the National Natural Science Foundation of China (30930077, 91027019, and 31000164), National Basic Research Program of China (2007CB925101), and Natural Science Foundation of Jiangsu Province (BK20130964).

REFERENCES

(1) Park, J.-H.; Gu, L.; Maltzahn, G. V.; Ruoslahti, E.; Bhatia, S. N.; Sailor, M. J. *Nat. Mater.* **2009**, *8*, 331−336.
(2) Erogbogbo, F.; Yong, K.-T.; Hu, R.; Law, W.-C.; Ding, H.; Chang, C.-W.; Prasad, P. N.; Swihart, M. T. *ACS Nano* **2010**, *4*, 5131−5138.
(3) Hessel, C. M.; Rasch, M. R.; Hueso, J. L.; Goodfellow, B. W.; Akhavan, V. A.; Puvanakrishnan, P.; Tunnel, J. W.; Korgel, B. A. *Small* **2010**, *6*, 2026−2034.
(4) Bimbo, L. M.; Mäkilä, E.; Laaksonen, T.; Lehto, V.-P.; Salonen, J.; Hirvonen, J.; Santos, H. A. *Biomaterials* **2011**, *32*, 2625−2633.
(5) Gu, L.; Park, J.-H.; Duong, K. H.; Ruoslahti, E.; Sailor, M. J. *Small* **2010**, *6*, 2546−2552.
(6) Anglin, E. J.; Cheng, L. Y.; Freeman, W. R.; Sailor, M. J. *Adv. Drug Delivery Rev.* **2008**, *60*, 1266−1277.
(7) Bimbo, L. M.; Sarparanta, M.; Santos, H. A.; Airaksinen, A. J.; Maklia, E.; Laaksonen, T.; Peltonen, L.; Lehto, V.-P.; Hirvonen, J.; Salonen, J. *ACS Nano* **2010**, *4*, 3023−3032.
(8) Xiao, L.; Gu, L.; Howell, S. B.; Sailor, M. J. *ACS Nano* **2011**, *5*, 3651−3659.
(9) Lee, C.; Kim, H.; Hong, C.; Kim, M.; Hong, S. S.; Lee, D. H.; Lee, W. I. *J. Mater. Chem.* **2008**, *18*, 4790−4795.
(10) Osminkina, L. A.; Tamarov, K. P.; Sviridov, A. P.; Galkin, R. A.; Gongalsky, M. B.; Solovyev, V. V.; Kudryavstev, A. A.; Timoshenko, V. Y. *J. Biophotonics* **2012**, *5*, 529−535.
(11) Sailor, M. J.; Wu, E. C. *Adv. Funct. Mater.* **2009**, *19*, 3195−3208.
(12) Wu, E. C.; Andrew, J. S.; Buyanin, A.; Kinsella, J. M.; Sailor, M. J. *Chem. Commun.* **2011**, *47*, 5699−5701.
(13) Hon, N. K.; Shaposhnik, Z.; Diebold, E. D.; Tamanoi, F.; Jalali, B. *J. Biomed. Mater. Res. Part A* **2012**, *100*, 3416−3421.
(14) Prtljaga, N.; Amato, E. D.; Pitanti, A.; Guider, R.; Froner, E.; Larcheri, S.; Scarpa, M.; Pavesi, L. *Nanotechology* **2011**, *22*, 215704.
(15) Chirvony, V.; Chyrvonaya, A.; Ovejero, J.; Matveeva, E.; Goller, B.; Kovalev, D.; Huygens, A.; Witte, P. *Adv. Mater.* **2007**, *19*, 2967−2972.
(16) Wang, J.; Liu, Y. X.; Peng, F.; Chen, C. Y.; He, Y. H.; Ma, H.; Cao, L. X.; Sun, S. Q. *Small* **2012**, *8*, 2430−2435.
(17) Xia, B.; Zhang, W.; Bao, W.; Dong, C.; Zhang, J.; Shi, J. S. *Phys. Status. Solidi A* **2012**, *209*, 2247−2250.
(18) Xia, B.; Zhang, W.; Shi, J. S.; Xiao, S. J. *Analyst* **2013**, *138*, 3629−3632.
(19) Karakoti, A. S.; Das, S.; Thevuthasan, S.; Seal, S. *Angew. Chem., Int. Ed.* **2011**, *50*, 1980−1994.
(20) Otsuka, H.; Nagasaki, Y.; Kataoka, K. *Adv. Drug Delivery Rev.* **2012**, *64*, 246−255.
(21) Kelf, T. A.; Sreenivasan, V. K. A.; Sun, J.; Kim, E. J.; Goldys, E. M.; Zvyagin, A. V. *Nanotechnology* **2010**, *21*, 285105.
(22) Liu, X. S.; Jin, Q.; Ji, Y.; Ji, J. *J. Mater. Chem.* **2012**, *22*, 1916−1927.
(23) Kairdolf, B. A.; Mancini, M. C.; Smith, A. M.; Nie, S. M. *Anal. Chem.* **2008**, *80*, 3029−3034.
(24) Breus, V. V.; Heyes, C. D.; Tron, K.; Nienhaus, G. U. *ACS Nano* **2009**, *3*, 2573−2580.
(25) Prencipe, G.; Tabakman, S. M.; Welsher, K.; Liu, Z.; Goodwin, A. P.; Zhang, L.; Henry, J.; Dai, H. J. *J. Am. Chem. Soc.* **2009**, *131*, 4783−4787.
(26) Yu, S. S.; Lau, C. M.; Thomas, S. N.; Jerome, W. G.; Maron, D. J.; Dickerson, J. H.; Hubbell, J. A.; Giorgio, T. D. *Int. J. Nanomed.* **2012**, *7*, 799−813.
(27) Zhang, B. B.; Wang, X. H.; Liu, F. J.; Cheng, Y. S.; Shi, D. L. *Langmuir* **2012**, *28*, 16605−16613.
(28) Aggarwal, P.; Hall, J. B.; McLeland, C. B.; Dobrovolskaia, M. A.; McNeil, S. E. *Adv. Drug Delivery Rev.* **2009**, *61*, 428−437.
(29) Mirkka, S.; Luis, M. B.; Jussi, R.; Ermei, M.; Timo, J. L.; Päivi, L.; Markus, N.; Jarno, S.; Markus, B. L.; Jouni, H.; Hélder, A. S.; Anu, J. A. *Mol. Pharmaceutics* **2012**, *9*, 654−663.
(30) Mahmoudi, M.; Lynch, I.; Ejtehadi, M. R.; Monopoli, M. P.; Bombelli, F. B.; Laurent, S. *Chem. Rev.* **2011**, *111*, 5610−5637.
(31) Yang, S. T.; Liu, Y.; Wang, Y. W.; Cao, A. N. *Small* **2013**, *9*, 1635−1653.
(32) Alain, W.; Mathieu, E.; Jacques, B. *Chem. Mater.* **2002**, *14*, 2757−2766.
(33) Rezwan, K.; Studart, A. R.; Voros, J.; Gauckler, L. T. *J. Phys. Chem. B* **2005**, *109*, 14469−14474.
(34) Xia, B.; Xiao, S. J.; Guo, D. J.; Wang, J.; Chao, J.; Liu, H. B.; Pei, J.; Chen, Y. Q.; Tang, Y. C.; Liu, J. N. *J. Mater. Chem.* **2006**, *16*, 570−578.
(35) Guo, D. J.; Xiao, S. J.; Xia, B.; Wei, S.; Pei, J.; Pan, Y.; You, X. Z.; Gu, Z. Z.; Lu, Z. H. *J. Phys. Chem. B* **2005**, *109*, 20620−20628.
(36) Serda, R. E.; Mack, A.; van de Ven, A. L.; Ferrati, S.; Dunner, K.; Godin, B.; Chiappini, C.; Landry, M.; Brousseau, L.; Liu, X. W.; Bean, A. J.; Ferrari, M. *Small* **2010**, *6*, 2691−2700.
(37) Bice, F.; Andrea, H. *Free Radical Biol. Med.* **2003**, *34*, 1507−1516.
(38) Fu, C. H.; Liu, T. L.; Li, L. L.; Liu, H. Y.; Chen, D.; Tang, F. Q. *Biomaterials* **2013**, *34*, 2565−2575.
(39) Liu, T. L.; Li, L. L.; Fu, C. H.; Liu, H. Y.; Chen, D.; Tang, F. Q. *Biomaterials* **2012**, *33*, 2399−2407.
(40) Liu, T. L.; Li, L. L.; Teng, X.; Huang, X. L.; Liu, H. Y.; Chen, D.; Ren, J.; Tang, F. Q. *Biomaterials* **2011**, *32*, 1657−1668.
(41) Huang, X. L.; Zhuang, J.; Teng, X.; Li, L. L.; Chen, D.; Yan, X. Y.; Tang, F. Q. *Biomaterials* **2010**, *31*, 6142−6153.
(42) Dmitri, K.; Minoru, F. *Adv. Mater.* **2005**, *17*, 2531−2544.
(43) Gennady, E. K.; Yury, A. K.; Igor, L. M.; Alexander, A. C.; Igor, N. *Phys. Chem. Chem. Phys.* **2012**, *14*, 13890−13902.
(44) Tasciotti, E.; Liu, X. W.; Bhavane, R.; Plant, K.; Leonard, A. D.; Price, B. K.; Cheng, M. M.-C.; Decuzzi, P.; Tour, J. M.; Robertson, F.; Ferrari, M. *Nat. Nanotechnol.* **2008**, *3*, 151−157.